

JPMTR 125 | 1905  
DOI 10.14622/JPMTR-1905  
UDC 655.1:537.5/530.1

Original scientific paper  
Received: 2019-03-07  
Accepted: 2019-09-15

# Nonlinear behavior in electrical properties of fully screen printed electroluminescent panels

Katrin Hirmer<sup>1</sup>, Christina Bodenstein<sup>2</sup>, Hans Martin Sauer<sup>2</sup>, Edgar Dörsam<sup>2</sup> and Klaus Hofmann<sup>1</sup>

<sup>1</sup>Technische Universität Darmstadt,  
Integrated Electronic Systems Lab,  
Merckstraße 25, 64283 Darmstadt, Germany

<sup>2</sup>Technische Universität Darmstadt,  
Institute of Printing Science and Technology,  
Magdalenenstr. 2, 64289 Darmstadt, Germany

katrin.hirmer@ies.tu-darmstadt.de  
bodenstein@idd.tu-darmstadt.de  
sauer@idd.tu-darmstadt.de  
doersam@idd.tu-darmstadt.de  
klaus.hofmann@ies.tu-darmstadt.de

## Abstract

We study the influences of printing parameters of fully screen printed electroluminescent panels on frequency and voltage dependent electrical properties of these devices. Significant nonlinear electrical features as well as a sensitivity to external illumination were observed. By varying the number of subsequent wet-in-wet printing steps within the dielectric and the luminescent layers of the electroluminescent panel, we studied the capacitive and dissipative behavior of current transport in the device. We used a novel method of high voltage impedance spectroscopy at frequencies between 10 Hz and 1 MHz with voltages up to 70 V<sub>rms</sub> and compared measurements taken in dark and illuminated ambiances. We propose a qualitative model on the nonlinearity based on ferroelectric and semiconductive features of the dielectric layers as described by the Drude model.

**Keywords:** printed electronics, printing parameters, high voltage impedance spectroscopy, AC powder electroluminescence, electroluminescent panel characterization

## 1. Introduction

Electroluminescent (EL) lighting technology is based on light emission from a luminescent material which is exposed to an alternating electric field. It is a non-thermal source of light which can be printed with a very low height. The EL panels are commonly produced by continuous coating techniques (Ranfeld, 2010). However, printing technology enables the efficient reproduction of structured layers by transferring a fluid from a printing form to a substrate with the advantage of printing specific structures in a cost-effective way.

In graphical printing technology, images are generated by superposition of dots with distinct primary colors (CMYK). The so-called raster dots must be small enough to create the impression of a continuous color. Thus, the focus in graphical printing is the color perception of the human eye. In contrast, the focus in printed electronics is on electrical properties, layer thickness and surface quality. The materials used for printed electronics are, for example, polymers, conduc-

tive or insulating materials which have to be printed continuously. Printed EL panels have already been created by screen printing (Sauer, Ranfeld, and Dörsam, 2010), flexographic printing (Ranfeld, Theopold and Dörsam, 2011), and pad printing technology (Lee, et al., 2010; Bodenstein, et al., 2018).

Compared to graphical printing, functional printing requires electrical characterization of the devices. Relations between printing parameters and electrical properties are of great interest to design the devices with respect to their electrical behavior. This paper focuses on the characterization of fully screen printed EL panels and draws conclusions to the printing parameters of the layer.

The paper is organized as follows: Section 2 explains the materials and methods which were used to print the EL samples. The printed panels are electrically characterized in Section 3. Section 4 discusses the findings of Section 3 and draws conclusions to the printing process. The overall paper is concluded in Section 5.

## 2. Printing process and materials

The EL panel is printed using the layer stack shown in Figure 1, starting with the electric rear electrode. As a substrate, we used PET, Hostaphan GN 4600 from Pütz Folien. Each layer requires material with specific properties, for example conductivity and transparency for the front electrode or isolating properties for the insulating layer. Each layer is printed, partially in several subsequent deposition steps and then dried before the next layer is printed on top of it.

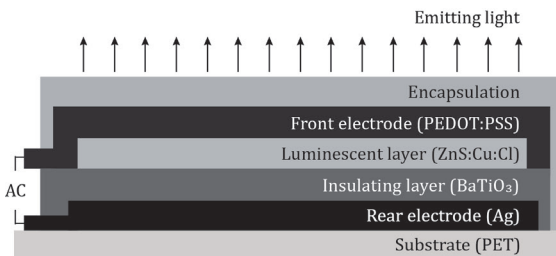


Figure 1: Schematic layer structure of the printed electroluminescent panels

Samples in other publications were partially screen printed onto a conductive precoated material or fabricated by spin coating or vacuum deposition (Kaiser, Marques and Correa, 2013; Kim, et al., 2011; Adachi, et al., 1988). The EL panels in this study were manufactured entirely by screen printing, using a semi-automatic flat screen printing machine K15Q SL from KBA Kammann GmbH.

In the present study, we used printing inks and materials, which could be physically (thermally) or chemically (UV) cured. The advantage of UV curable materials is the low, almost negligible shrinkage in the curing process, and a fast-continuing processing compared to solvent based ink.

For later validation of the electrical parameters, we considered two different EL panel sizes, 16 cm<sup>2</sup> and 4 cm<sup>2</sup> of the luminescent area, each disk and square shaped. Processing parameters were identical since all four layouts were printed in the same printing run. We used commercially available screen printing UV inks for the insulating and the luminescent layer. For the former, the ink consists of ferroelectric BaTiO<sub>3</sub> particles dispersed in a varnish, with a solid content of 50 %. As the luminescent layer, zinc sulfide ZnS:Cu:Cl particles were processed in a widely used UV binder and optimized for screen printing. A solvent-based material was used for the rear electrode, whereas the transparent front electrode was made using an aqueous dispersion. A thermal curing process of 20 min. was necessary for drying the electrode material.

Meshes with a stencil thickness of 8–12 μm of emulsion over the mesh, and a mesh cover angle of 22.5° were used. Printing and drying were done at approximately 23 °C at 50 % relative humidity. The hot air oven (HAO) used for drying, took its air inflow from this atmosphere as well, with an air exhaust flow of 140 m<sup>3</sup>h<sup>-1</sup>. The used printing inks and related screen parameters are listed in Table 1.

Table 1: Processing materials used for screen printed electroluminescent samples

Layer	Material (ink)	Mesh material	Mesh count [1/cm]	Mesh thread diameter [μm]
Rear electrode	Ag (Electrodag PF050)	metal	95	36
Insulating layer	BaTiO <sub>3</sub> (Elantas EL7030)	polyester	64	64
Luminescent layer	ZnS:Cu:Cl (Elantas 7001)	polyester	100	40
Front electrode	PEDOT:PSS (EasyCon P3145)	polyester	140	34
Encapsulation	Dupont encapsulant	polyester	100	40

Table 2: Processing parameters used for screen printed electroluminescent samples

Layer	Printing velocity [m/s]	Squeegee hardness [Shore A]	Drying conditions	# Printing steps	
				Batch 1	Batch 2
Rear electrode	0.4	55	HAO: 120 °C 20 min	1	1
Insulating layer	0.4	75	UV: 70 % 15 m/min	1–4	2
Luminescent layer	0.1	75	UV: 70 % 15 m/min	2	1–4
Front electrode	1.0	75	HAO: 100 °C 20 min	3	3
Encapsulation	0.3	65	HAO: 100 °C 20 min	2	2

The processing parameters such as printing velocity, squeegee hardness, drying conditions and the number of repeated printing steps, which were used for specific layers, are listed in Table 2. They largely follow the recommendations of the manufacturer and proved to be satisfactory for defect-free printing.

The dielectric and the luminescent layers were built up by a sequence of several subsequent printing steps. The ink of each subsequent step was printed on the preceding layer before it had solidified, i.e. layer deposition consisted of multiple wet-in-wet steps. Subsequently, the layer was dried according to Table 2. In this way, we created panels with different insulating and luminescent layer thicknesses and thus distinct electrical properties.

For studying the influence of the insulating layer thickness, we varied the number of wet-in-wet printing steps of the insulating material from one to four using two printing steps for the luminescent layer (Batch 1). In order to study the influence of the luminescent layer thickness, the number of printing steps was defined analogously for the respective layers (Batch 2).

Also here, the subsequent steps were deposited without intermediate drying. Both insulating and luminescent layers were cured in a drying conveyor oven system by IST with UV radiation spectrum of 180–450 nm. The curing power was set to 70 % of the nominal maximal power of 8.0 kW. Finally, an encapsulation layer was added for insulation and protection against air and humidity, using a solvent based material printed on top of the multilayer stack. In order to measure the insulating layer thicknesses resulting from the different numbers of subsequent wet-in-wet printing runs, appropriate samples were printed separately on the PET substrate. The thickness was determined using a tactile profilometer DektakXT from Bruker with a pin radius of 2.5  $\mu\text{m}$  and a stylus force of 3 mg.

### 3. Results

The fully screen printed EL samples were characterized with respect to electrical as well as luminance parameters. Particular attention was paid to the relationship between the characterized values and printing parameters.

#### 3.1 Influence of printing parameters on luminance

For full characterization of the EL panels, an inverter platform was specifically developed in order to control the parameters of the electrical excitation. A maximum output peak-to-peak voltage of up to 400  $V_{pp}$  with any required output waveform could be obtained for frequencies up to 5 kHz (Hirmer, et al., 2016). Compared

to other available inverters (Goncharov, et al., 2017; Assef, et al., 2013), the developed inverter platform can change significantly more parameters and thus characterize the EL panels more extensively.

The luminance, light emission per area in  $\text{cd}/\text{m}^2$ , was measured with a Gossen MavoMonitor for sinusoidal shaped excitation voltages. As expected, the measurements verified that the luminance is independent of size and shape of the panels. The measurements henceforth were concentrated to one specific layout, a square-shaped panel with an area of 16  $\text{cm}^2$ . It was found that at least two steps for the insulating layer were necessary to safely avoid pinholes and thus short circuits. We observed that printing the insulating layer in only one step yielded to an imprint of the screen, which can be avoided by printing two steps.

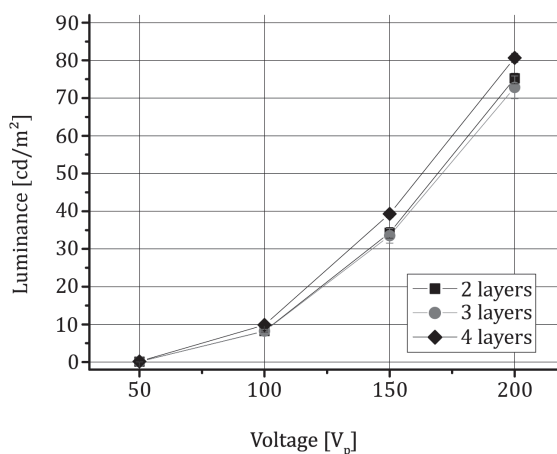


Figure 2: Influence of  $\text{BaTiO}_3$  insulating layer thickness on luminance for sinusoidal peak voltage ( $V_p$ ) waveforms of 5 kHz

We focused on samples with two to four subsequent depositing steps for the insulating layer. As expected, the results of the luminance measurements showed that the luminance was increasing with voltage (see Figure 2).

Table 3: Measured layer thicknesses for the number of printed  $\text{BaTiO}_3$  insulating layers

# Printing steps	Layer thickness (average) [ $\mu\text{m}$ ]
1	25.1 ( $\pm 1.4$ )
2	46.5 ( $\pm 4.1$ )
3	53.1 ( $\pm 6.3$ )

Table 3 shows that the insulating layer thickness is increasing with the number of subsequent printing steps as a function of the number of subsequent wet-in-wet printing. There are two additional observations: Firstly, the ink transfer ratio from the screen

to the substrate, i.e. the increment in layer thickness, became smaller with each repetition. Layer thickness was not a linear function of the number of printing steps. Secondly, the average deviation of the mean layer thickness, i.e. the surface roughness, became gradually larger at the same time. We would have expected that the leveling of the wet printed layer by surface tension was more efficient when layer thickness is large. Apparently, the opposite is true here: leveling of irregularities and smoothing of the surface became worse. We attribute this to a progressing aggregation of the BaTiO<sub>3</sub> particles in the ink, making the material more and more immobile.

Despite the increase of the thickness of the insulating layer with the number of printing steps, the capacitance per area did not increase as expected. In particular, it should be inversely proportional to the thickness values shown in Table 3. Figure 2 shows the influence of two, three and four printed insulating layers on the luminance with sinusoidal excitation peak voltages from 50 V<sub>p</sub> to 200 V<sub>p</sub> at 5 kHz. One observes a voltage at V<sub>0</sub> ~50 V<sub>p</sub> below which there was no light emission.

Above this voltage, luminance increases with  $(V - V_0)^2$  where  $V$  is the operation voltage. This indicates some nonlinearity in the electro-optical behavior of the panel, specifically at voltages close to  $V_0$ . Interestingly, luminance does not significantly change with number of printing steps, and with the dielectric layer thickness. In view of the thickness measurements, one would have expected that capacitance per area and thus luminance decreased. Contrary to this expectation, the maximum of luminance, although being only marginal, was observed with four printed insulating layers (with highest applied voltage of 200 V<sub>p</sub> and a frequency of 5 kHz). This interesting phenomenon has important implications on process design and on the structure of equivalent electrical circuits for EL technology. A similar effect has also been reported in an earlier work for pad printed panels (Bodenstein, et al., 2019). Here, this was assigned to an increasing compactification of the porous BaTiO<sub>3</sub> layer with the number of subsequent deposition steps. This aspect will be discussed in Section 4.

### 3.2 High voltage impedance characterization of electroluminescent panels

Figure 3a shows a complex electrical equivalent circuit model which takes account of the electric features related to the different printed layers (Ono, 1995). The model is intended for the low frequency range. Here, the nonlinear behavior can be observed. The nonlinearities can be assigned to D<sub>1</sub> and D<sub>2</sub> and R<sub>D</sub>. This part represents the luminescent layer which can be regarded as a short circuit in lighted condition. For

voltages above V<sub>0</sub> as reported in Section 3.1, a simplified electrical equivalent model as shown in Figure 3b can be used for the inverter design. In lighted condition, the EL panel can be regarded as a serial connection of a resistor R<sub>PEDOT</sub>, which is related to the transparent front electrode and a parallel connection of C<sub>EL</sub> and R<sub>EL</sub>.

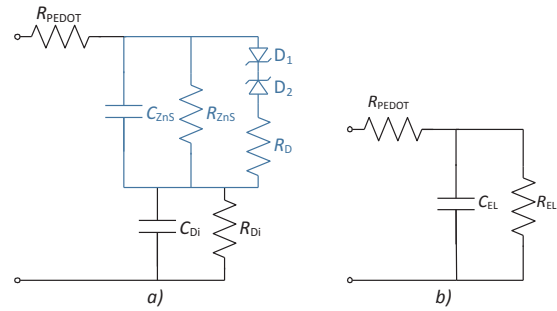


Figure 3: Equivalent circuit of an electroluminescent panel: (a) complex model for off-condition, (b) simplified model for on-condition, since D<sub>1</sub>, D<sub>2</sub> and R<sub>D</sub> can be neglected in lighted condition; adapted from Ono (1995)

The values for all components of the equivalent circuit can be extracted from impedance measurements. Therefore, all printed panels were characterized with a ModuLab® XM MTS system (AMETEK Scientific Instruments, n.d.). It can measure the impedances of the EL panels with average (root mean square) voltages up to 70 V<sub>rms</sub> (≈ 200 V<sub>pp</sub>). Hence, contrary to most characterizations in literature, the panels can be tested above the threshold voltage of the luminescence layer in lightning conditions, i.e. in the nonlinear range. Figure 4 shows exemplarily the Bode plot of a 16 cm<sup>2</sup> disk EL panel with two layers of insulation in off-condition (1 V<sub>rms</sub>) and on-condition (70 V<sub>rms</sub>).

Compared to previous measurements (Ionescu, Drăghici and Bonfert, 2015; Kaiser, Marques and Correa, 2013), the frequency range can be expanded to higher frequencies achieving a better electronic understanding of the panel. Higher frequency characterization is of particular interest if the EL is excited with non-sinusoidal pulse sequences, or if the stray capacitors are of importance, e.g. in capacitive proximity sensors (Hirmer, Saif and Hofmann, 2018).

Figure 4 shows the panel impedance and the phase as a function of operating frequency between 10 Hz and 1 MHz, measured with a low voltage amplitude of 1 V<sub>p</sub> (such that the panel is dark), and with 70 V<sub>p</sub> (such that the panel is bright). We observe a decrease in impedance for frequencies below ~200 Hz for the bright panel, and an even more substantial phase difference of up to 6° at frequencies below ~10 kHz. Table 4 summarizes these voltage-dependent effects which were extracted at 1 kHz, a typical operation fre-

quency for EL panels. This feature can be assigned to the activation of the bright luminescent layer and is taken in account in the equivalent circuit by the non-linear elements of the ZnS layer.

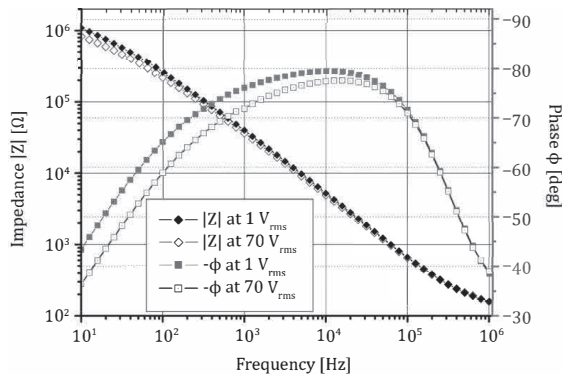


Figure 4: Measured impedance of an EL panel in off ( $1 V_{rms}$ ) and on condition ( $70 V_{rms}$ )

Table 4: Comparison of the impedance measurement at  $1 V_{rms}$  and  $70 V_{rms}$  at 1 kHz

Voltage [ $V_{rms}$ ]	Impedance [ $\Omega$ ]	Phase [ $^\circ$ ]
1	39870.0	-76.1
70	34630.0	-71.9
Ratio	-15.1 %	-5.9 %

The impedance measurement verifies that the impedance of an EL panel cannot be entirely characterized by a capacitor with a serial resistor. A parallel resistor is required as well. It reflects the feature that the phase tends to  $0^\circ$  at  $\omega \rightarrow 0$ .

### 3.3 Influence of the $BaTiO_3$ insulating layers on the impedance

As described in Section 2, the EL panels from Batch 1 were printed with up to four different layers of  $BaTiO_3$  insulation to investigate the influence of the insulating layer on the overall performance of the panel. As expected, the thickness of the insulating layer is increasing with the number of printed layers (though not in a linear manner, see Table 3).

Following the physics of a parallel plate capacitor, the capacitance is expected to decrease with increasing layers of insulating material. However, measurements in lighted condition ( $70 V_{rms}$ ) revealed a converse behavior as shown in Figure 5. For the sake of comparability, the capacitance was extracted at 100 kHz since the permittivities of the materials are specified by the manufacturer for this frequency. It can be seen that the measured mean capacitance is increasing with the number of insulating layers for all shapes and sizes of the EL panels.

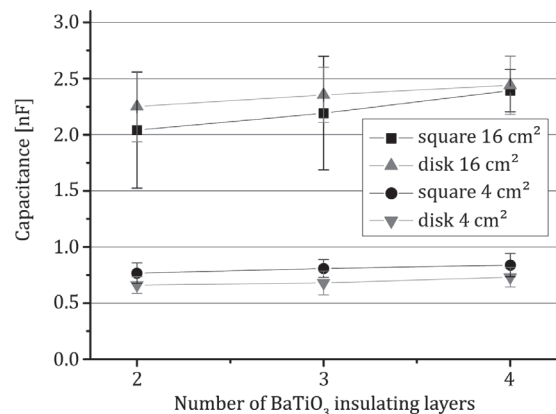


Figure 5: Measured mean capacitance of all printed panels increases with the number of printed  $BaTiO_3$  insulating layers

Whereas the thickness is increasing by 14.29 % from two to three layers of insulation, the capacitance is slightly increasing by 7.42 % for  $16 \text{ cm}^2$  large square-shaped EL panels. This could be attributed to an increasing compactness of the underlying insulating layer by the additional printing steps. This effect will be discussed in more detail in Section 4.

### 3.4 Influence of ambient light condition on capacitance measurement

In addition to the influences of printing parameters, we observed that the panel capacitance also depended on the ambient illumination of the panel. Panel capacitance is tentatively smaller under dark than under illuminated condition, but the tendency is not that reproducible in the dark as compared to the illuminated case. With the high voltage impedance measurement equipment, the effect of ambient light can be verified quantitatively. The measured impedances were fitted to the equivalent circuit model shown in Figure 3b with a major focus on  $C_{EL}$  and  $R_{PEDOT}$ . These two parameters were extracted for on- and off-conditions of the EL at different ambient illumination, i.e. in a dark and a bright environment. The comparison of the extracted capacitance and resistance was referenced to the capacitance value of the high voltage measurement at bright condition  $C_{EL}(70 V_{rms,bright})$  since the EL panel is typically used in lighted environments. Hence, this impedance represents the load that the inverter has to drive.

The comparisons of the different operating conditions of the EL measurement setup are shown in Table 5. Compared to the reference  $C_{EL}(70 V_{rms,bright})$ , the high voltage measurement in the dark does not show significant influences on capacitance. This can be explained by the light emitted by the panel itself (see column 1 in Table 5).

Table 5: Comparison of the measured capacitance at different ambient light conditions and the reference capacitance  $C_{EL,ref}$  being  $C_{EL}(70 V_{rms,bright})$

	$\frac{C_{EL}(70 V_{rms,dark}) - C_{EL,ref}}{C_{EL,ref}}$	$\frac{C_{EL}(1 V_{rms,bright}) - C_{EL,ref}}{C_{EL,ref}}$	$\frac{C_{EL}(1 V_{rms,dark}) - C_{EL,ref}}{C_{EL,ref}}$
Square 16 cm <sup>2</sup> [%]	-6.5	+46.4	-13.9
Disk 16 cm <sup>2</sup> [%]	-5.3	+40.8	+4.5
Square 4 cm <sup>2</sup> [%]	-6.2	+49.6	-16.5
Disk 4 cm <sup>2</sup> [%]	-6.3	+42.0	-2.0

Measuring the capacitance at low voltages shows an excess of capacitance  $\Delta C$  up to 50 % compared to 70  $V_{rms}$  bright conditions (see column 2 in Table 5). Measurements with low voltages at dark conditions still show a discrepancy of up to -16 % (see column 3 in Table 5). However, this difference is considerably smaller than at bright conditions. Consequently, if only a low voltage capacitance or impedance meter is available, the capacitance of the EL should be characterized in dark conditions (compare Table 5).

For the inverter design, the series resistance  $R_{PEDOT}$  is the second important parameter since it determines the maximum current that has to be delivered by the output stage of the inverter. Measurements showed that the resistance can be determined at any voltage, i.e. low or high voltage, and any ambient condition, i.e. dark or bright, leading to a maximum standard deviation of 2.6 %.

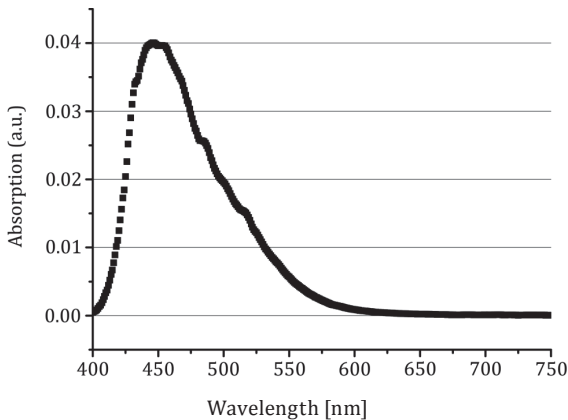


Figure 6: Absorption spectrum of the screen printed electroluminescent panels with a peak at 446 nm

It can be concluded that the operation condition has an enormous influence on the extracted capacitance. We found that ambient light is responsible for this systematic deviation. The absorption spectrum of the screen printed EL panels was measured with a spectrometer, NanoCalc from OceanOptics, Largo, USA. From this it follows that the absorption wavelength peak range center is measured at 446 nm which is in the visible range of light wavelength (see Figure 6).

As molecular absorption and emission of photons are always interconnected, this could explain the origin of the electron-hole-excitation in the luminescent layer which contributes to its polarizability in the electric field. If the EL impedance is measured at voltages which are high enough to excite fluorescence in the ZnS, the absorption of photons from ambient light contributes only few compared to the number of electrically induced electron-hole-pairs. Consequently, ambient light has only little influence on the impedance of the panel. If the device is measured at low voltages, i.e. below the threshold voltage  $V_0$ , no electron-hole-pairs can be created by the electrical field. Therefore, the pairs from absorption of ambient photons provide the majority of mobile charge carriers. Hence, ambient light has significant effect on the electrical parameters at low voltage characterization. For this reason, EL panels should be characterized at dark ambient conditions.

### 3.5 Influences of luminescent layers on capacitance

As described in Section 2, a second series of EL samples was produced, varying the number of ZnS:Cu:Cl luminescent layers (one to four) with constant number of printing steps of the BaTiO<sub>3</sub> insulating layer (Batch 2). These EL panels enabled investigations of the luminescent layers on the electrical parameters.

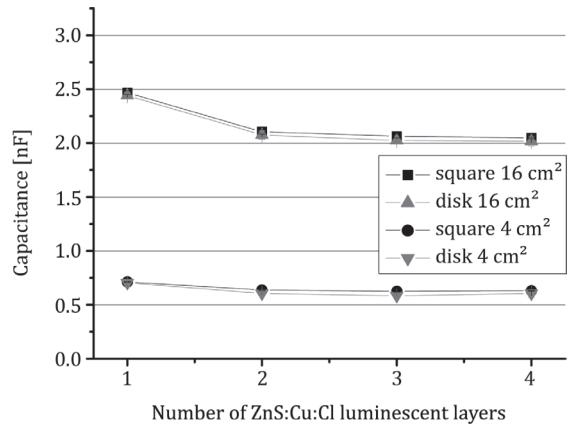


Figure 7: Measured mean capacitance of all printed panels decreases with the number of printed luminescent layers

Figure 7 shows the change of capacitance with increasing number of luminescent layers. It can be seen that the capacitance is slightly decreasing with each deposited layer, in contrast to the tendency found when varying the printing steps of the insulating BaTiO<sub>3</sub> layer where the capacitance is increasing (compare Figure 5). We assign this to the feature that solid ZnS particles have a much lower permittivity than BaTiO<sub>3</sub> particles. The permittivity  $\epsilon_r$  of ZnS is of order of 6 (Madelung, Rössler and Schulz, 1999), whereas it is of order of 1000 (Adachi, et al., 2001) and more for ferroelectric BaTiO<sub>3</sub> particles. Thus, even if ZnS particles agglomerate in the printed layer as shown in Figure 8, the effect on the total dielectric constant of the layer and thus on capacitance should be much smaller in this case. The increase of layer thickness dominates here the effect of a possible particle compactification within the layer.

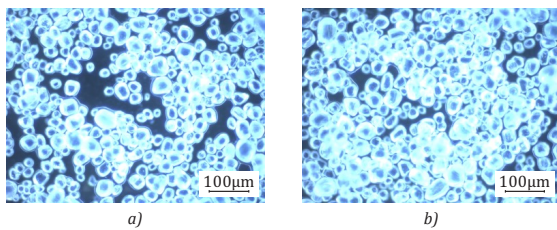


Figure 8: Fluorescent microscopic images of printed layers of ZnS particles for (a) one and (b) two printing steps

Regarding the structure of the EL panel as shown in Figure 1, the capacitance  $C_{EL}$  of the EL is composed by two series capacitances. One is determined by the insulating layer and one is determined by the luminescent layer. Hence, the overall capacitance can be calculated by

$$\frac{1}{C_{EL}} = \frac{1}{C_{Insulating}} + \frac{1}{C_{Luminescent}} \quad [1]$$

with the capacitance  $C_i$  with  $i$  indicating insulating and luminescent, respectively. By using a parallel plate approach,  $C_i$  can be calculated using the printing and material data by

$$C_i = \frac{\epsilon_0 \epsilon_{r,i} A}{d_i} \quad [2]$$

with  $\epsilon_0$  being the vacuum permittivity,  $\epsilon_{r,i}$  being the relative permittivity of the material  $i$ ,  $A$  being the area and  $d_i$  being the thickness of the layer. The relative permittivities  $\epsilon_r$  of the printed composite materials at 100 kHz are given by the manufacturer to 7.5 for the insulation and 3.5 for the luminescent layer, respectively. Using an EL area  $A$  of 16 cm<sup>2</sup>, the measured layer thicknesses of Table 3 and a luminescent layer thickness of 51.0 µm, the capacitances can be calculated by Equation [2] and compared to the measured values.

For the square-shaped panel with three printing steps of luminescent layers, it can be seen that the discrepancy of the measured values compared to the calculated series connection  $C_{EL}$  is more than 63 % (see penultimate row of Table 6). We tried to extract the reciprocal relative permittivity  $1/\epsilon_{r,Luminescent}$  from our data and obtained values close to or even below zero. Regarding the error bars, this may be interpreted as an electrical conductive interlayer with  $\epsilon_{r,Luminescent} \rightarrow \infty$ . Comparing the calculated capacitances  $C_{Insulating}$  to the measurement results in a failure of down to 5.9 %, which proves the statement above (see bottom row of Table 6).

Table 6: Comparison of calculated and measured capacitances for 16 cm<sup>2</sup> square-shaped panels with three printing steps of the luminescent layer

	min	mean	max
Calculated $C_{Insulating}$ [nF]	1.79	2.00	2.27
Calculated $C_{Luminescent}$ [nF]	0.95	0.97	0.99
Calculated $C_{EL}$ [nF]	0.62	0.65	0.69
Measured $C_{measured}$ [nF]	1.69	2.19	2.70
$\frac{C_{measured} - C_{EL}}{C_{measured}}$ [%]	63.19	70.17	74.40
$\frac{C_{measured} - C_{Insulating}}{C_{measured}}$ [%]	-5.89	8.77	15.81

#### 4. Discussion

The electrical impedance of printed EL panels depends on and hence can be designed by the manufacturing process of the different layers of the panel stack. The front electrode, i.e. its limited electrical sheet conductivity, has a foreseeable and well understood impact and can be accounted for by a series resistor  $R_{PEDOT}$  in our electrical low-frequency impedance model. Manufacturing details of the insulating and the luminescent layers show quite unexpected effects. Even more surprising was the significance of nonlinear electrical panel behavior in our experiments. Its impedance depends significantly on the operation voltage and even on the light exposure of the panel.

It was shown that the capacitance of the panel is a function of the number of subsequently printed insulating layers. We did not always observe a decrease in capacitance and light emission when the layer thicknesses were increased. For the insulating BaTiO<sub>3</sub> layer, we could indeed verify that multiple wet-in-wet overprinting increased the final layer thickness. However, no decrease in panel capacitance was found. We assign this to a progressing compactification of the BaTiO<sub>3</sub> particles in the layer. Even if this compactification was

small from the point of view of layer morphology, the dielectric effect could be significant because the specific dielectric polarizability of barium titanate is extremely large compared to the binder polymer. Even a small reduction of porosity of the particle network dispersed in the UV curable polymer varnish should yield a large increase in the overall  $\epsilon_r$  of the compound. For the printing process, this implies that wet-in-wet application of additional material will not only increase the layer thickness but may also affect the morphology of the particulate network in the already deposited fraction of the layer. This may, in case of high  $\epsilon_r$ -powders such as BaTiO<sub>3</sub>, result in an increased polarizability, compensating the effect of the increasing layer thickness. Using dispersions of only small or average polarizability such as ZnS, this latter effect may be unrecognized. This interpretation also explains the increase of light emission that was observed in panels made with multiple insulating layer printing steps (see Figure 2).

Considering the luminescent ZnS layer, another effect appears. Although panel capacitance decreased with the thickness of the ZnS layer as qualitatively expected, the capacitor exhibited voltage- and radiation-related sensitivities. Our experiments clearly imply that this must be related to the ZnS not to the BaTiO<sub>3</sub> layer. Increasing operation voltage from 1 V<sub>rms</sub> to 70 V<sub>rms</sub> in a frequency range between 10 Hz and ~10 kHz revealed an additional dielectric loss. The phase  $\Phi(\omega)$  significantly decreased from the low voltage value by ~6°. The point here is not that the phase is higher than -90° as one would expect for a capacitor with loss-free dielectrics, but rather that the observed loss angle found at low operation voltage increased when switching to high voltages. One also finds some effect in the absolute impedance  $|Z(\omega)|$ , but this is small and may easily escape under the measurement noise.

We represented the nonlinearity in our equivalent electrical circuit model by two inversely oriented Zener diodes D<sub>1</sub> and D<sub>2</sub> as shown in Figure 3a. In addition, two resistors R<sub>D</sub> and R<sub>ZnS</sub> are provided to describe the impedance of the device. The Zener diodes represent the threshold voltage V<sub>0</sub> associated with the onset of light emission of the EL panel. This is explained in Figure 2.

Physically this means, that the contribution of the luminescent layer to dielectric polarizability disappears as soon as light emission is active. The ZnS apparently behaves more like a conductor than like a polarizable insulator and it virtually appears to be no longer present in the capacitor. In this state, the BaTiO<sub>3</sub> layer seems to be the only dielectric layer as calculations in Table 6 show. This behavior could be explained by the electron-hole pairs which are excited across the band gap of ZnS in the electric field. These electron-hole pairs are responsible for light emission

by their recombination. Charge carrier recombination takes some time which is of order of few nanoseconds, typically. In this period, however, they contribute to current transport. The excited ZnS exhibits a small but finite conductivity (Kobayashi, et al., 1973; Kaiser, Marques and Correa, 2013), comparable to the conductivity of e.g. ionic electrolytes.

According to the Drude model of electron-related conduction in solids, this corresponds to a dielectric constant with a frequency-dependent imaginary part, i.e.

$$\epsilon_r(\omega) \sim 1 + i \frac{\omega_p^2 \tau}{\omega} \quad [3]$$

where  $\omega_p$  is the excitation frequency of the electron-hole pair and  $\tau$  is the characteristic life time of the excited state. The Drude model allows to calculate the phase difference  $\Delta\Phi(\omega)$  between the non-excited state (where the free charge carrier related fraction of the imaginary part of  $\epsilon_r$  vanishes) and the excited state. This is given by

$$\tan \Delta\phi(\omega) \sim \frac{\omega_p^2 \tau}{\omega} \quad [4]$$

and implies that the phase difference should scale as 1/ω and disappear with increasing frequency. This was qualitatively confirmed by the measurements (see Figure 4). For these reasons, thickness and layer porosity of the luminescent layer drop out of the specific capacitance in the on-state of the panel. They are still of some relevance in the off-state.

Electron-hole pairs can also be created in zinc sulfide by optical absorption. This feature is an evident characteristic of luminescent ZnS in contrast to nonluminescent materials like BaTiO<sub>3</sub> as was used in the insulating layer. It explains the observed nonlinear dependence of electrical impedance, namely of the parallel resistances on the illumination of the panel.

## 5. Conclusions

This work focuses on the nonlinear behavior of fully screen printed electroluminescent panels. For the first time, investigations showed the influences of high voltage characterization in comparison to low voltage characterization. From the impedance measurements it can be concluded that the impedance of an electroluminescent panel changes depending on operation voltage and illumination due to the activation of the ZnS:Cu:Cl luminescent layer. This effect is most pronounced at lowest frequencies when one compares impedance measurements taken at low and at high voltages. In doing so, the ambient light is absorbed within the luminescent layer. Furthermore, the high voltage impedance measurement showed that the

thickness of luminescent layer and its morphology is almost insignificant for the overall capacitance of the panel in contrast to the features of the insulating layer.

The measurements imply that an increase in insulating layer thickness leads to a decrease of porosity of that layer which in turn increases the capacitance of the fully screen printed electroluminescent panels. For the first time, the high voltage measurement of

complex impedance showed the differences of on- and off-condition of the electrical parameters of electroluminescent panels. Our experiment indicates that electroluminescent panels, when adequately driven with alternating voltages, could also be interesting alternatives for printed optical or radiation sensors, since photon absorption and pair creation in the ZnS layer can immediately be detected in a characteristic change of the electrical properties.

## Acknowledgement

The authors would like to acknowledge the support by Franz Binder GmbH & Co. to make their luminance measurement system available and Henkel Electronic Materials for providing silver ink used in this work.

## References

- Adachi, C., Tokito, S., Tsutsui, T. and Saito, S., 1988. Electroluminescence in organic films with three-layer structure. *Japanese Journal of Applied Physics*, 27(2A), pp. L269–L271. <https://doi.org/10.1143/JJAP.27.L269>.
- Adachi, M., Akishige, Y., Asahi, T., Deguchi, K., Gesi, K., Hasebe, K., Hikita, T., Ikeda, T., Iwata, Y., Komukae, M., Mitsui, T., Nakamura, E., Nakatani, N., Okuyama, M., Osaka, T., Sakai, A., Sawaguchi, E., Shiozaki, Y., Takenaka, T., Toyoda, K., Tsukamoto, T. and Yagi T., 2001. BaTiO<sub>3</sub> (hexagonal) [F] Survey, 1A-10. In: Y. Shiozaki, E. Nakamura and T. Mitsui, eds. *Ferroelectrics and related substances: oxides*. Berlin, Heidelberg: Springer Verlag. <https://doi.org/10.1007/b53034>.
- AMETEK Scientific Instruments, n.d. *ModuLab XM MTS – Materials Test System*. [online] Available at: <<http://www.ameteksi.com/products/materials-testing-systems/modulab-xm-mts>> [Accessed 06 March 2019].
- Assef, A.A., Maia, J.M., Schneider, F.K., Button, V.L.S.N. and Costa, E.T., 2013. A reconfigurable arbitrary waveform generator using PWM modulation for ultrasound research. *Biomedical Engineering OnLine*, 12: 24. <https://doi.org/10.1186/1475-925X-12-24>.
- Bodenstein, C., Sauer, H.M., Dörsam, E. and Hirmer, K., 2018. Influence of printing parameters in fully pad-printed electroluminescence panels on curved surfaces. In: *19<sup>th</sup> International Society of Coating Science and Technology Symposium (ISCST)*. Long Beach, CA, USA, 16–19 September 2018.
- Bodenstein, C., Sauer, H.M., Hirmer, K. and Dörsam, E., 2019. Printing process and characterization of fully pad printed electroluminescent panels on curved surfaces. *Journal of Coatings Technology and Research (online first)*.
- Goncharov, I.N., Kabyshev, A.M., Kozyrev, E.N. and Maldzigaty, A.I., 2017. Power source for electroluminescent panels. *Journal of Communications Technology and Electronics*, 62(6), pp. 634–637. <https://doi.org/10.1134/S1064226917060080>.
- Hirmer, K., Saif, M.B. and Hofmann, K., 2018. Integrated symmetrical high voltage inverter for the excitation of touch sensitive electroluminescent devices. In: *2018 IEEE 30<sup>th</sup> International Symposium on Power Semiconductor Devices and ICs (ISPSD 2018)*. Chicago, IL, USA, 13–17 May 2018. Piscataway, NJ, USA: IEEE, pp. 343–346.
- Hirmer, K., Schuster, P., Keil, F. and Hofmann, K., 2016. Low-cost high-voltage arbitrary waveform generator for broad lifetime measurements of electroluminescent devices. In: *2016 2<sup>nd</sup> Annual Southern Power Electronics Conference (SPEC 2016)*. Auckland, New Zealand, 5–9 December 2016. Piscataway, NJ, USA: IEEE, pp. 155–158.
- Ionescu, C., Drăghici, F. and Bonfert, D., 2015. A SPICE model for electroluminescent foils. In: *2015 38<sup>th</sup> International Spring Seminar on Electronics Technology (ISSE 2015)*. Eger, Hungary, 6–10 May 2015. Piscataway, NJ, USA: IEEE, pp. 526–531.
- Kaiser, W., Marques, R.P. and Correa, A.F., 2013. Light emission of electroluminescent lamps under different operating conditions. *IEEE Transactions on Industry Applications*, 49(5), pp. 2361–2369. <https://doi.org/10.1109/TIA.2013.2260315>.
- Kim, J.-Y., Bae, M.J., Park, S.H., Jeong, T., Song, S., Lee, J., Han, I., Yoo, J.B., Yung, D. and Yu, S., 2011. Electroluminescence enhancement of the phosphor dispersed in a polymer matrix using the tandem structure. *Organic Electronics*, 12(3), pp. 529–533. <https://doi.org/10.1016/j.orgel.2010.12.020>.
- Kobayashi, H., Tanaka, S., Sasakura, H. and Hamakawa, Y., 1973. The electron injection mechanism of the electroluminescent ZnS: Tb<sup>3+</sup> films. *Japanese Journal of Applied Physics*, 12(12): 1854. <https://doi.org/10.1143/JJAP.12.1854>.
- Lee, T.-M., Hur, S., Kim, J.-H. and Choi, H.-C., 2010. EL device pad-printed on a curved surface. *Journal of Micromechanics and Microengineering*, 20(1): 015016. <https://doi.org/10.1088/0960-1317/20/1/015016>.

- Madelung, O., Rössler, U. and Schulz, M. eds., 1999. Zinc sulfide (ZnS) dielectric constant, cubic modification. In: *Landolt-Börnstein – Group III Condensed Matter 41B (II-VI and I-VII Compounds; Semimagnetic Compounds)*. Berlin, Heidelberg: Springer Verlag. [https://doi.org/10.1007/10681719\\_392](https://doi.org/10.1007/10681719_392).
- Ono, Y.A., 1995. *Electroluminescent displays*. Singapore: World Scientific Publishing. <https://doi.org/10.1142/2504>.
- Ranfeld, C., 2010. *Drucktechnische Herstellung eines funktionalen Demonstrators*. Diplomarbeit. Technische Universität Chemnitz.
- Ranfeld, C., Theopold, A. and Dörsam, E., 2011. Flexographic printing for the production of inorganic electroluminescent devices. In: *Proceedings of Printing Future Days 2011: 4<sup>th</sup> International Scientific Conference on Print and Media Technology*. Chemnitz, Germany, 7–10 November 2011. Berlin: VWB Verlag.
- Sauer, H.M., Ranfeld, C. and Dörsam, E., 2010. An investigation of the screen printing process for electroluminescent panels and the influence of printing parameters on the performance of the panels. In: *Electronics Convention proceedings, LOPE-C 2010 scientific paper: LOPE-C, Large-Area, Organic & Printed Electronics Convention: International Conference and Exhibition for the Organic and Printed Electronics Industry*. Frankfurt, Germany, 31 May–2 June 2010. Frankfurt, Germany: OE-A.